Ocean Dynamics (2003) 53: 323–331
DOI 10.1007/s10236-003-0041-z

Simon J. Marsland · Mojib Latif · Stephanie Legutke

Antarctic circumpolar modes in a coupled ocean–atmosphere model

Received: 18 June 2002/Accepted: 20 May 2003

Abstract Eastward-propagating patterns in anomalous potential temperature and salinity of the Southern Ocean are analyzed in the output of a 1000-year simulation of the global coupled atmosphere–ocean GCM ECHO-G. Such features can be associated with the so-called Antarctic Circumpolar Wave (ACW). It is found that time–longitude diagrams that have traditionally been used to aid the visualization of the ACW are strongly influenced by the width of the bandpass time filtering. This is due to the masking of considerable low-frequency variability that occurs over a broad range of time scales. Frequency–wavenumber analysis of the ACW shows that the eastward-propagating waves do have preferred spectral peaks, but that both the period and wavenumber change erratically when comparing different centuries throughout the simulation. The variability of the ACW on a variety of time scales from interannual to centennial suggests that the waiting time for a sufficient observational record to determine the time scale of variability of the real world ACW (and the associated decadal time scale predictability of climate for southern landmasses) will be a very long one.

Keywords AOGCM · Antarctic Circumpolar Wave · Southern Ocean · Coupled Model

1 Introduction

Observational studies have suggested the existence of an Antarctic Circumpolar Wave (ACW) at the ocean–atmosphere interface of the Southern Ocean (Jacobs and Mitchell 1996; White and Peterson 1996). The observed ACW is characterized by a wavenumber-2 pattern with eastward-propagating anomalies. Since the ACW has a signature in both the ocean (sea-surface temperature, sea-surface elevation) and the atmosphere (sea-level pressure, meridional wind stress), it was hypothesized by White and Peterson (1996) that the ACW represents a coupled ocean–atmosphere mode. Variability associated with this mode is found to have a period of 4–5 years, indicating a time scale of 8–10 years for circumpolar transits of the signal. However, the available observations are of limited duration, resulting in poor resolution of spectral characteristics of the data at low frequencies, and visualization of the ACW has also relied on the use of bandpass filtering of the data with a relatively narrow window with respect to the interannual time scales being investigated.

Spatial and temporal sparsity of observations is by no means unique to the Southern Ocean, although it is more conspicuous there than elsewhere. Hence, coupled general circulation models (CGCMs) of the ocean and atmosphere have been applied to the study of the ACW to facilitate greater understanding. Christoph et al. (1998) identified an ACW mode using 180 years of mean monthly output from the ECHAM4/OPYC3 coupled model. The main differences between their modeled ACW and that observed were the predominance of wavenumber 3 in the model and the standing, rather than propagating, nature of the atmospheric anomalies. However, the apparent discord between the ECHAM4/OPYC3 model and observations may, in fact, be due to the short time period of the observations used, as Bonekamp et al. (1999) showed that for the ECMWF reanalysis period atmospheric anomalies associated with the ACW shifted from a standing pattern early on to a propagating pattern at around the beginning of the period analyzed by White and Peterson (1996). Cai et al. (1999), using 60 years of mean monthly output from the CSIRO coupled model, also noted the prevalence of standing features in the atmospheric component of the ACW. In that study it was shown that the propagating oceanic anomalies were in resonance with a standing wavenumber-3 atmospheric forcing pattern similar to

Responsible Editor: Dirk Olbers

S. J. Marsland (✉) · M. Latif · S. Legutke
Max-Plank-Institute für Meteorologie, 2650095 Bundesstr. 55, 20146, Hamburg, Germany
e-mail: marsland@dkrz.de
Tel.: +49 (0)40-41173-244
Fax: +49 (0)40-41173-298

that identified by Mo and White (1985), leading Cai et al. (1999) to the conclusion that the ACW may represent a coupled ocean–atmosphere mode even when atmospheric anomalies are not propagating.

One purpose of this study is to highlight that a degree of uncertainty remains concerning the acceptance of such a mode in the real or modeled climate system. In particular, we stress that the observational evidence spans the time scale of only one single complete ACW realization, and that GCM simulations of ACW-like phenomena have also relied to some extent on the use of time domain bandpass filtering that, by construction, displays variability only on and about the ACW time scale. As it turns out, we find that in addition to the interannual variablity, that can be described as an ACW, a considerable amount of background variability exists at lower frequencies with no preferred spectral peaks. The results, however, should be interpreted with caution. Like many other OAGCMs including an active sea-ice component, the ECHO-G model has a relatively poor simulation of Southern Ocean sea ice, characterized by widespread open-ocean convection and large scale polynyas. Unfortunately, long time scale integrations (order 1000 years) with realistic Southern Ocean sea ice are not currently available.

Specifically, we use the output of a 1000-year simulation of a coupled ocean–atmosphere–sea-ice model to explore the variability of the frequency and wavenumber characteristics of the ACW in time. In Section 2 a brief description of the component models, the coupling strategy, and the experiment are given. In Section 3 the effects of time domain filtering on visualization of the ACW are highlighted, and the erratic nature of the low-frequency variability of the ACW is investigated. A discussion and conclusions are given in Section 4.

2 Model description

The model used in this study is the ECHO-G coupled ocean–atmosphere model as described by Legutke and Voss (1999). The atmospheric component is ECHAM-4 (Roeckner et al. 1996), the Hamburg version of the ECMWF operational model, at T30 spectral truncation with 19 levels. The ocean component is the Hamburg Ocean Primitive Equation (HOPE) model (Wolff et al. 1997) at a resolution approximating T42L20 with equatorial grid refinement. The grid refinement produces relatively high meridional resolution (0.5° latitude) over a band from 10°N to 10°S, and is intended for the purposes of modeling ENSO variability in the tropical Pacific Ocean. Details of the ocean grid formulation and of the climatology of the ocean model's response to the ECHAM4 atmospheric fluxes are given by Legutke and Maier–Reimer (1999). The ECHO-G coupled model has previously been used in studies of the variability of the Indian (Baquero–Bernal et al. 2002) and the tropical Pacific (Rodgers et al. 2000) Oceans. It is a descendant of the ECHO model which was used in studies of decadal variability in the Pacific (Latif and Barnett 1994) and Atlantic (Grötzner et al. 1998) Oceans. A major difference between ECHO-G and ECHO is the inclusion of a thermodynamic–dynamic sea-ice model employing the viscous plastic rheology of Hibler (1979).

Prior to coupling, both component models of ECHO-G, the ocean and the atmosphere, were spun up separately. The surface conditions (SST, sea-ice thickness and concentration, and snow cover over sea ice) used in the 18-year spin-up of the atmosphere model have been obtained by a stand-alone integration of the ocean model which includes the sea-ice calculation. Fluxes at the lower boundary of the atmosphere are calculated separately over water and ice, as described by Grötzner et al. (1996).

The models are coupled with the help of the OASIS coupling software developed at CERFACS (Terray et al. 1998), which also handles the interpolation between the approximate T42 (with equatorial refinement) Ocean grid and the T30 atmosphere grid. The mismatch between ocean and atmosphere resolutions is a trade-off between highest possible resolution with available computing resources and the computational requirements of the component models.

The flux corrections are calculated in a 155-year coupled spin-up integration where the SST was restored to climatological monthly data with a time scale corresponding to 40 W m^{-2} K^{-1}. SSS was restored to annual mean values. No restoring, however, was done in the ice regions (defined by monthly climatologies) to let the freezing and melting process of sea ice freely determine the salinity and thus stability beneath the sea ice. Annual mean heat and freshwater flux correction fields are diagnosed from the last 100 years of the 155-year spin-up integration, and then applied throughout the 1000-year coupled integration. This approach minimizes biasing associated with the initial shock to the component systems due to mismatches in the fluxes used to force the stand-alone ocean and atmosphere components in the spin-up integrations prior to coupling, and the associated mismatches in the mean states of the spun-up component models. Judged from surface variables such as near-surface or sea-surface temperatures or sea-ice extent, the 1000-year run was very stable after an initial adjustment to the new forcing conditions (global mean temperature increase was 0.1×10^{-2} °C per 100 a).

3 Results

As has been done with observations (White and Peterson 1996) and CGCMs (Christoph et al. 1998; Cai et al. 1999) we construct time–longitude diagrams of time-filtered anomalies averaged over a constant latitude band. Figure 1 shows time–longitude diagrams of sea-surface temperature and salinity anomalies (SSTA and SSSA, respectively). To allow comparison with the CSIRO CGCM of Cai et al. (1999), the latitude band 46–65°S and a 1–10-year bandpass filter are chosen. For

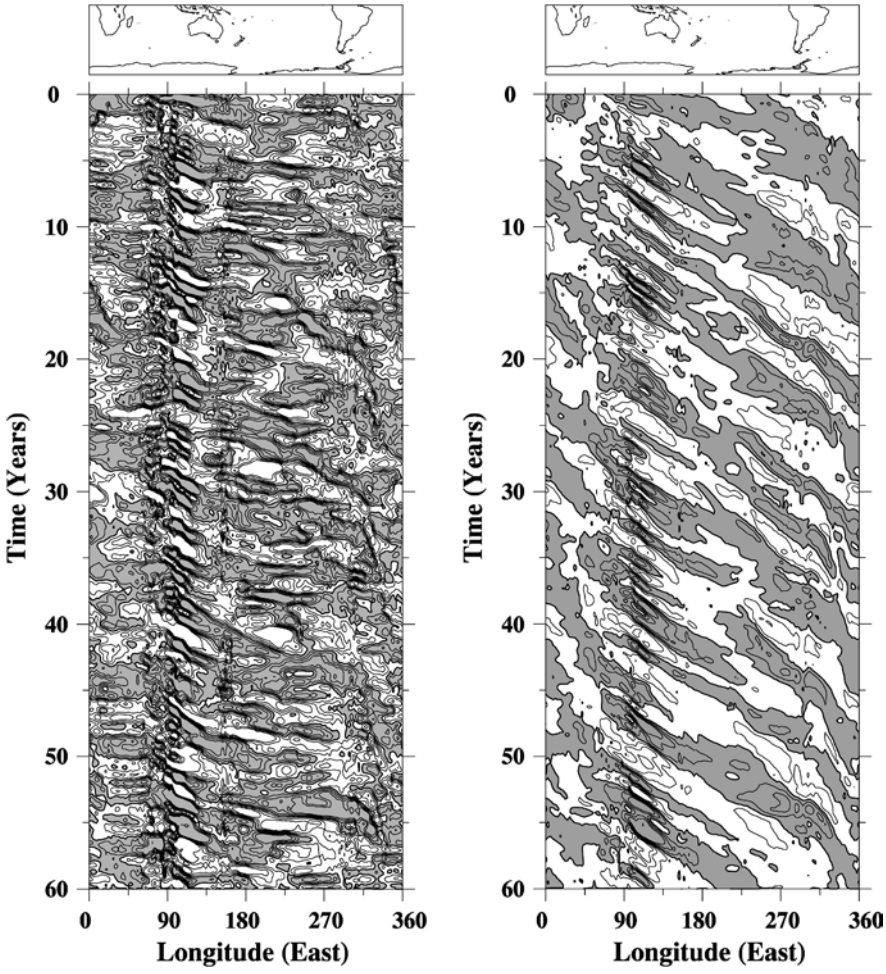

Fig. 1 One–10-year bandpass filtered Hovmoeller diagrams of mean monthly SSTA (*left*) and SSSA (*right*) over the first 60 years of the simulation. Values are averaged over the latitude range 46–65°S. Contour interval is 0.1 °C for temperature and 0.1 psu for salinity, with negative values *shaded*. The *far left panels* are simply to assist visualization

increased clarity, only the first 60 years are plotted, although the anomalies were calculated with respect to the first 100 years of the simulation. A much longer time period could have been chosen from which to calculate anomalies. However, this introduces effects associated with very low-frequency changes in local mean state. That is, local anomalies with respect to the full 1000 years may not change sign for periods of 60 years or more. The SSSA plot is qualitatively comparable to the time–longitude diagram of SSTA shown by Christoph et al. (1998) and the subsurface equivalents of Cai et al. (1999). The same cannot be said for the SSTA, which could better be described as very noisy. Indeed, it is difficult to see any clear signal of ACW, like propagation or associated time scale, in the SSTA signal. This is attributed to the fact that the upper-layer thickness in the ECHO-G model is only 20 m, as opposed to the use of the entire mixed layer to determine the SSTA signal in the isopycnal model of Christoph et al. (1998).

A much clearer picture of the eastward propagation of both salinity and temperature can be seen in the deeper (and thicker) subsurface layers, as shown in Fig. 2. Only the salinity anomalies are shown here, but it is noted that the patterns of temperature anomalies are very similar. There are two important features discernable in Fig. 2: firstly, that the magnitude of anomalies attains a maximum in two regions, in the SE Indian Ocean near 90°E and in the SE Pacific Ocean near 270°E; and secondly, that the propagation rate of the patterns is reduced with depth.

The existence of preferred regions of anomaly generation (or maxima) in the ECHO-G model is similar to both observations and other model studies. However, the locations of these regions tend to vary somewhat between studies. Largest SSTAs are found in the central Pacific region of the Southern Ocean by both White and Peterson (1996) and Christoph et al. (1998), while the model of Cai et al. (1999) shows maxima further east and also in the Indian Ocean sector. In the ECBilt model, anomalies appear strongest in a region stretching from the eastern Pacific into the Atlantic Ocean (Haarsma et al. 2000). The maxima in the ECHO-G ACW anomalies in the Indian Ocean occur in a region of persistent open-ocean convection and weak vertical stratification in the model, resulting in too-warm sea-surface temperatures and very little sea-ice formation along the East Antarctic coastline, especially from 90–135°E. The same behavior can be seen in the uncoupled ocean model forced with ECHAM4 surface

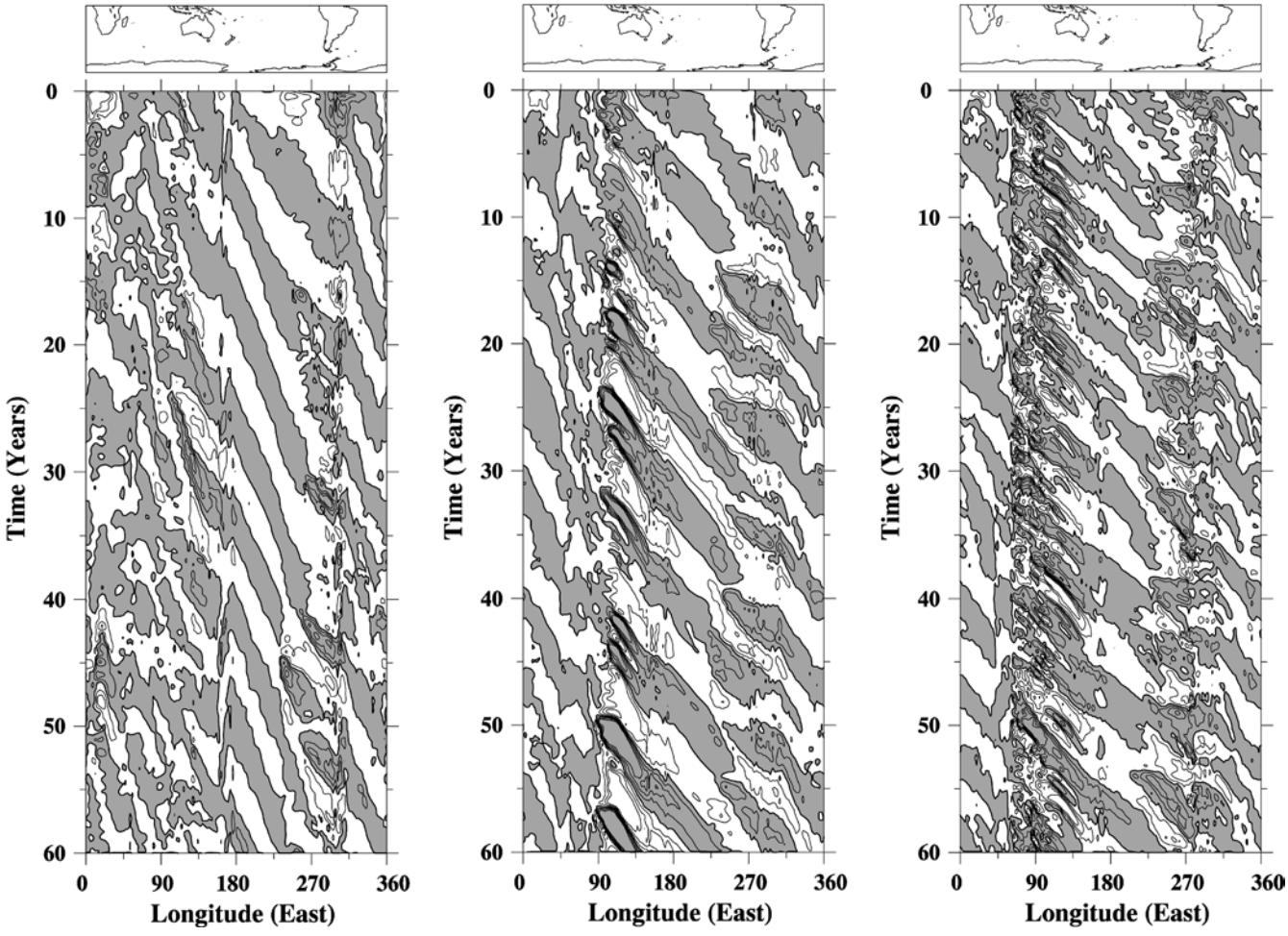

Fig. 2 One–10-year bandpass filtered Hovmoeller diagrams of mean monthly salinity anomalies for model layers 225–275 m (*right* C.I. = 0.02 psu), 500–700 m (*middle* C.I. = 0.02 psu), and 900–1200 m (*left* C.I. = 0.005 psu)

fluxes (Legutke and Maier–Reimer 1999) derived from an atmospheric run with AMIP SST. There, the strong convection results from the southeastward advection of warm and saline subtropical Indian Ocean water via the Agulhas Current into the Antarctic Circumpolar Current (ACC). The relaxation of SST in particular is based on the rather zonal AMIP SST in the Southern Ocean, and consequently works hard to restore this zonality. Since the southeastward advection of warm and saline subtropical Indian Ocean water is not a model artifact, there is some physical argument that the heat flux (and hence the ACW signal) is large in that region. However, although the variability is not necessarily overestimated, the mean heat flux in this region is. While the oscillation in the strength of the resultant convection is responsible for the large anomalies in both salinity and temperature in the ECHO-G ACW, it remains unclear what determines the time scale. The mechanism responsible for creating the maxima in the ECHO-G ACW anomalies in the SE Pacific Ocean remains unclear.

The reduction of ACW propagation rate with depth in ECHO-G is in contrast to the results from the CSIRO model as reported by Cai et al. (1999), where it was found that the ACW had a barotropic nature to the mid depths of the ocean. The baroclinic nature of the oceanic component of the ACW in ECHO-G seems to support the advective-resonance theory proposed by Weisse et al. (1999). Since the zonal velocity of the ACC reduces with depth, the advection of anomalies downstream from regions of generation should also reduce with depth, as evidenced by the increased slope of the features in the time–longitude diagrams of Fig. 2. Hovmoeller diagrams of atmospheric fields (sea-level pressure, surface-air temperature) were qualitatively similar to those of SST (see Fig. 1), with no evidence of coherent standing or propagating patterns. Therefore, it remains unclear whether the advective-resonance or coupled ocean–atmosphere explanation of an ACW should be favored based on the current study.

Bandpass filtering has been routinely used for the identification of an ACW in both observations (White and Peterson 1996; 3–7-year filter) and models (Christoph et al. 1998: 1–20-yea r filter; Cai et al. 1999: 1–10-year filter); Bonekamp et al. 1999: 1–7-year filter). Comparison with unfiltered anomalies has not previously appeared in the literature, raising the question of to what extent the filtering may affect the analysis or simply the visualization of the ACW. Figure 3 gives an

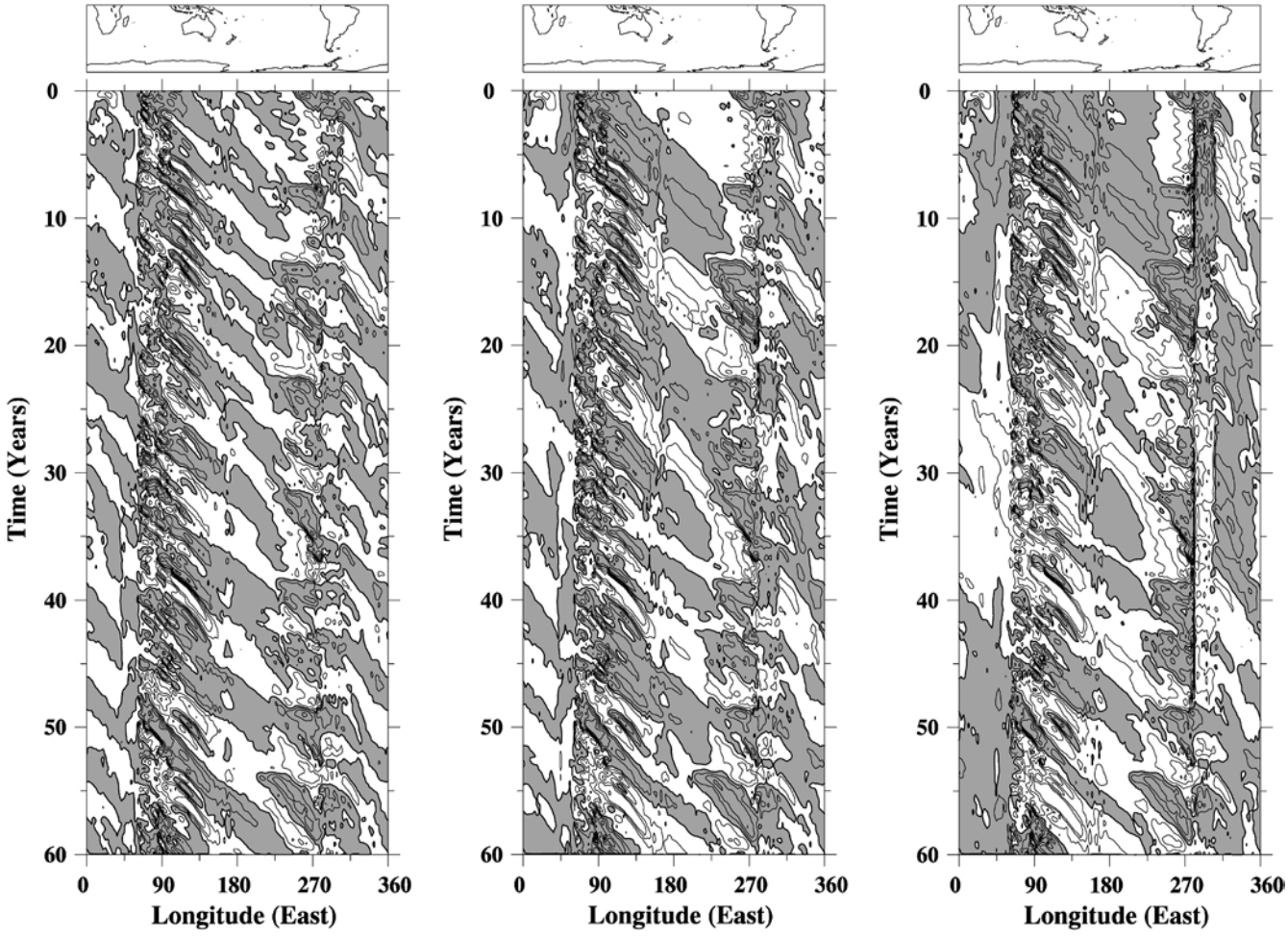

Fig. 3 Hovmoeller diagrams of mean monthly salinity anomalies in model layer 225–275 m. Unfiltered anomalies (*right*), 1–20-year bandpass filtered anomalies (*middle*), and 1–10-year bandpass filtered anomalies (*left*)

example of the effects of bandpass filtering on the construction of time–longitude diagrams. As can be seen when comparing Fig. 3 to the bottom panel of Fig. 2, there is a considerable amount of low-frequency detail removed from the unfiltered signal, raising the question of whether the ACW phenomenon may be as much a figment of the time filtering as a representation of any real ocean mode. For example, in the region 0–45°E the unfiltered variability appears to be better characterized by a multidecadal oscillation (approximately 20-year time scale) than by an interannual oscillation. Although the filtered anomalies show a much clearer signal of circumpolar eastward propagation, it can also be seen that the width of the filter affects the time scale of the modeled ACW. This is particularly apparent in the regions 135–225°E and 315–360°E (i.e., downstream from the two identified regions of anomaly generation), where the ACW time scale is reduced with decreasing filter width. For example, at 180°E there are six periods of negative (shaded) anomalies when using a 1–20-year filter, compared to nine periods when using a 1–10 year filter. While the use of time-domain filtering is a common and justifiable practise in the study of climate variability, we feel that it is also important that any effects of such filtering, such as the considerable refinement of the model ACW signal, should be made clear.

If indeed there is a real ocean mode that can be associated with the ACW, it is reasonable to expect some evidence of it in a frequency–wavenumber analysis of the unfiltered anomalies. White and Peterson (1996) did this with the observational data and found a clear peak in the range of 4–5 years. However, noting that they used a maximum of $N = 156$ months (13 years) of mean monthly data, they could then only resolve periods of N/M for M in $\{1,2,\ldots, N/2\}$ using the Fourier decomposition in time. Therefore, in the low-frequency range they could only resolve periods at 13 years (the fundamental frequency of the available data), 6.5, 4.33, 3.25, 2.6, etc. years. This poor resolution of the frequency domain allows for a reasonable suspicion of the validity of the ACW time scale obtained. With the much longer time series (180 years) available from the model of Christoph et al. (1998), dominant peaks were reported at both wavenumbers 2 and 3 with a period slightly over 4 years, although closer inspection of their figure shows that the dominant peaks are the two wavenumber-1 peaks between 6- and 8-year periods.

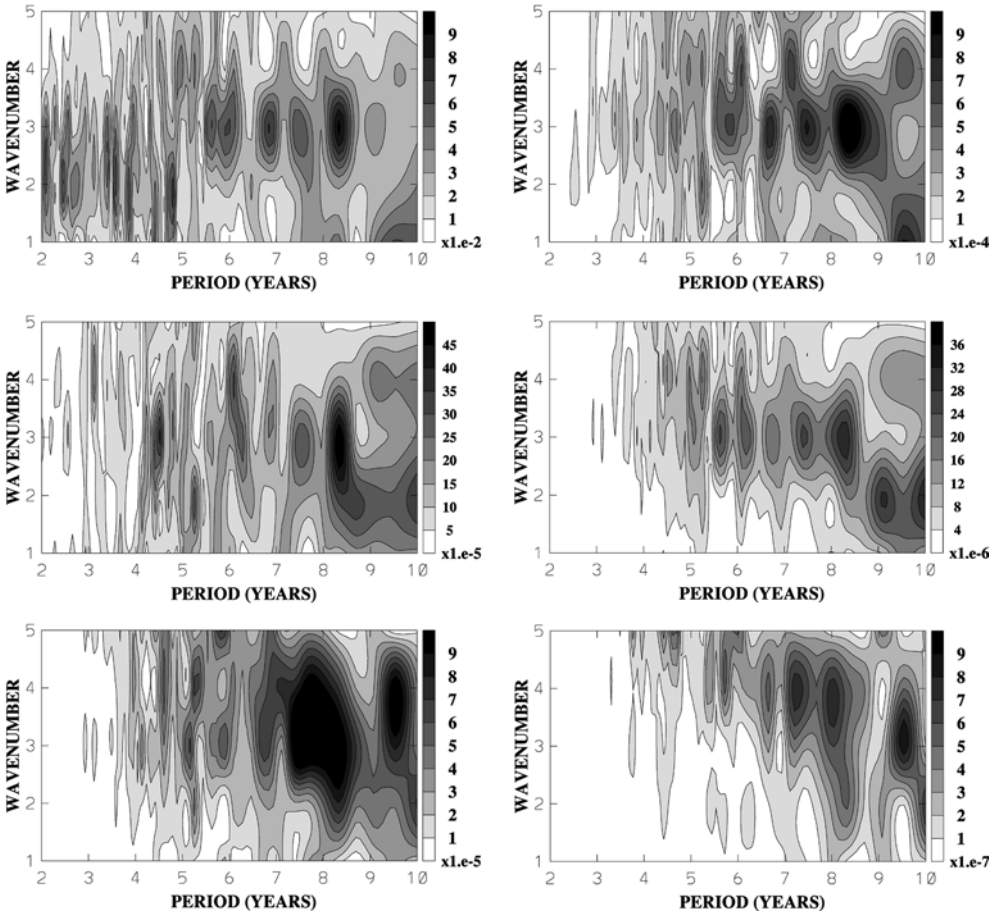

Fig. 4 Frequency–wavenumber diagrams of net ocean–atmosphere heat flux (*upper left*), potential energy release by convection (*upper right*), SST (*middle left*), SSS (*middle right*), 225–275 m temperature (*bottom left*), and 225–275 m salinity (*bottom right*). Each analysis was performed using 1000 years of unfiltered mean monthly output, with units of units^2 month^{-1} appropriate to each field (e.g., salinity in psu^2 month^{-1}). Scaling factors are indicated at the *lower right of the bars*

Figure 4 shows frequency–wavenumber spectra of a variety of surface fields along with temperature and salinity for the 225–275-m layer. One noticeable feature is the occurrence of a wavenumber-3 peak having a period of slightly over 8 years in all of the surface fields shown. However, the corresponding circumpolar transit time of around 25 years is not easily associated with the model's ACW as depicted in the previously shown time–longitude diagrams. For the deeper layer, peak spectral powers in temperature are at both wavenumbers 3 and 4 in the 7.5- to 8.5-year period band, and also at wavenumber 4 with a 9-year period. For salinity the periods of peak variance power are similar, although only at wavenumber 4 for the 7.5- and 8.5-year periods, and at wavenumber 3 instead of 4 for the 9.5-year period.

The frequency–wavenumber analysis was repeated for each of the 10 centuries of the simulation, with the results for salinity in the 225–275-m layer shown in Fig. 5. As can be seen, there is a large degree of variability in the frequency–wavenumber characteristics between centuries. In centuries 1, 3, and 6 both wavenumbers 2 and 4 dominate, although the period varies between centuries. Wavenumbers 2 and 4 also appear to dominate in century 2 but the peak power is greatly reduced here. Wavenumber 3 is dominant in centuries 7 and 10, while maxima are at wavenumbers 3 and 4 in centuries 4 and 9. For centuries 5 and 8 peak power occurs at wavenumber 4.

The similarity between time–longitude diagrams of temperature and salinity in subsurface model layers that was reported above suggests that the frequency–wavenumber analysis for temperature in the 225–275-m layer should be similar to that of Fig. 5. However, comparison of the period and wavenumber of the peak power of temperature was found to correspond with salinity in only half of the 10 centuries analyzed (figure not shown). Repeating this analysis for other model layers indicated that peak powers were more likely to be of higher wavenumbers (3 and 4) in deeper layers of the model and lower wavenumbers (2 and 3) in layers nearer the surface. This is consistent with the idea of two regions of anomaly generation (SE Indian and SE Pacific) and reduced eastward propagation with depth, as shown in Fig. 2.

4 Discussion

An important caveat to consider when interpreting the results of this study is the inability of the model to reproduce the observed state of the high-latitude Southern Hemisphere coupled ocean/sea-ice system. In

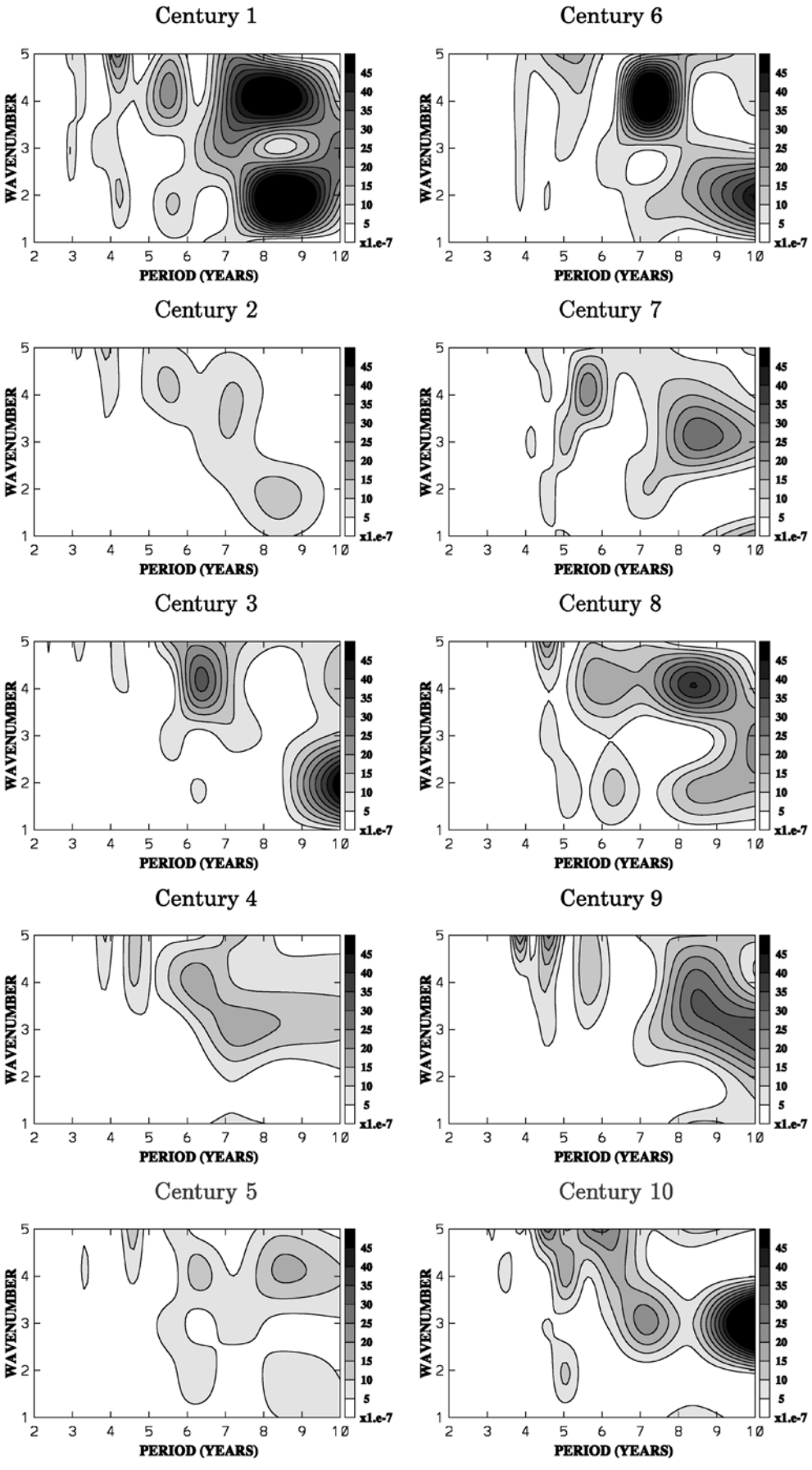

Fig. 5 As in Fig. 4 but for salinity in the 225–275-m layer, where the frequency–wavenumber spectrum is calculated separately for each of the 10 centuries in the 1000-year simulation

particular, the ECHO-G simulation underestimates both Antarctic sea-ice extent and thickness. Furthermore, open-ocean deep convection in the Southern Ocean is excessive and widespread and results in large-scale open-ocean polynyas. These problems are common to many OAGCMs that include sea ice, and they significantly affect water masses and circulation (e.g., strength of the ACC). This is in discord with the limited observations available, and is known to have considerable influence on the watermass characteristics of intermediate and deep waters.

In this study, it was found that an oceanic mode of variability exists in the ECHO-G simulation that can be identified with the so-called ACW. The patterns of easterly propagation are found from the surface to a depth of over 1000 m. Both the magnitude of anomalies and the rate of propagation reduce with increasing depth. Two questionable aspects of the interpretation of statistical analyses with respect to the ACW have been raised. Firstly, to a large extent the visualization of the ACW relied on the use of bandpass filtering in time. It is noted that such filtering has been widely used in previous studies. The time-filtering was shown to mask lower-frequency variability, and in its absence the existence of an ACW in ECHO-G was by no means certain. Indeed, the discrepancy between the filtered and unfiltered signals gives some indication as to why a clear 4–5-year cycle of variability has not previously been detected in the much longer time series of station data from both Antarctica and the extremities of the southern continents. Secondly, the intercentennial comparison of the frequency–wavenumber analyses showed that there is considerable variability in both the spatial and temporal scales of the ACW. Variability in the spatial scales of the atmospheric forcing over the Southern Ocean has previously been identified by Bonekamp et al. (1999) within the ECMWF reanalysis fields on decadal time scales. Using the much longer dataset available from our coupled model, variability can also be identified in the frequency of the ACW signal. The erratic nature of the modeled ACW on longer time scales suggests that, rather than being a single mode, the variability in the Southern Ocean may better be described as a superposition of many Antarctic circumpolar modes operating on a variety of time scales.

It has been suggested (White and Cherry 1999) that the ACW may provide a possible source of seasonal predictability. It is also reasonable to expect that a well-known ACW mode would be useful for prediction of seasonal sea-ice extent, concentration, and thickness variability. However, if the erratic nature of variability having multiple time scales as seen in the ECHO-G model is representative of the natural system, this seems unlikely for decadal time-scale applications. The situation is further frustrated because the time history of available observations is simply inadequate for resolving the power spectra at periods beyond a couple of years. Nevertheless, the increasing availability of satellite and other observations in the Southern Ocean does suggest that our knowledge of the current state will improve with time. This allows for some optimism with regards to seasonal time-scale predictions, provided that we can firstly identify the current strength and location of oceanic ACW-like features, and secondly differentiate between a propagating or standing wave atmospheric response.

There is no reason to expect that the ECHO-G coupled experiment is any more or less successful a representation of the natural climate than the models of, for example, Christoph et al. (1998) or Cai et al. (1999). Although the results from this study do not confirm or deny that the ACW is not a persistent and real climate mode, they do offer evidence that a reasonable degree of uncertainty exists in the results of observational and modeling efforts that have attempted to qualify and quantify such a mode. Hence, they provide a valid reason for considerable caution in interpreting the results from the limited studies constituting the available literature to date. Both more extensive observations and more realistic models are required before the ACW mode can be considered as a likely source of information with respect to predictability, for example, of interannual climate variability for the extreme Southern Hemisphere landmasses.

Acknowledgements The CGCM was integrated on a NEC SX-4 in a joint project of MPI and NEC European Supercomputer Systems, NEC Deutschland GmbH. We thank the staff of NEC for their support in carrying out the 1000-year simulation. Thanks are also due to the staff of CERFACS, who made the OASIS coupling software available and helped with the installation of the model on the NEC machine. We also acknowledge the support from the staff of DKRZ for setting up the coupled model and supervising the integration, and we thank Reiner Schnur for assistance with the frequency–wavenumber software. Finally, we are grateful to two anonymous reviewers for their comments and criticisms.

References

Baquero-Bernal A, Latif M, Legutke S (2002) On dipole-like variability of sea-surface temperature in the tropical Indian Ocean. J Climate 15: 1358–1368

Bonekamp H, Sterl A, Komen GJ (1999) Interannual variability in the Southern Ocean from an ocean model forced by European Centre for Medium-Range Weather Forecasts reanalysis fluxes. J Geophys Res 104(C6): 13317–13331

Cai W, Baines PG, Gordon HB (1999) Southern mid- to high-latitude variability, a zonal wavenumber-3 pattern, and the Antarctic Circumpolar Wave in the CSIRO coupled model. J Climate 12: 3087–3104

Christoph M, Barnett TP, Roeckner E (1998) The Antarctic Circumpolar Wave in a coupled ocean–atmosphere GCM. J Climate 7: 1659–1672

Grötzner A, Sausen AR, Clausen M (1996) The impact of sub-grid scale sea-ice imhomogenities on the perfomance of the atmospheric general circulation model ECHAM3. Clim Dyn 12: 477–496

Grötzner A, Latif M, Barnett P (1998) A decadal climate cycle in the North Atlantic Ocean as simulated by the ECHO coupled GCM. J Climate 11: 831–847

Haarsma RJ, Selten FM, Opsteegh JD (2000) On the mechanism of the Antarctic Circumpolar Wave. J Climate 13: 1461–1480

Hibler WD (1979) A dynamic thermodynamic sea-ice model. J Phys Oceanogr 9: 815–846

Jacobs GA, Mitchell JL (1996) Ocean circulation variations associated with the Antarctic Circumpolar Wave. Geophys Res Lett 23: 2947–2950

Latif M, Barnett TP (1994) Causes of decadal climate variability over the North Pacific and North America. Science 266: 634–637

Legutke S, Maier-Reimer E (1999) Climatology of the HOPE-G global ocean general circulation model. Technical Report 21, German Climate Computer Center (DKRZ)

Legutke S, Voss R (1999) The Hamburg atmosphere–ocean coupled circulation model ECHO-G. Technical Report 18, German Climate Computer Center (DKRZ)

Mo KC, White GH (1985) Teleconnections in the Southern Hemisphere. Mon Weath Rev 113: 22–37

Rodgers KB, Latif M, Legutke S (2000) Sensitivity of equatorial Pacific and Indian Ocean water masses to the position of the Indonesian throughflow. Geophys Res Lett 27: 2941–2944

Roeckner E, Arpe K, Bengtsson L, Christoph M, Claussen M, Dümenil L, Esch M, Giorgetta M, Schlese U, Schulzweida U (1996) The atmospheric general circulation model ECHAM-4: model description and simulation of present-day climate. Technical Report 218, Max Planck Institute for Meteorology

Terray L, Valcke S, Piacentini A (1998) The oasis coupler user guide. Version 2.2. Technical Report TR/CMGC/98-05, CERFACS

Weisse R, Mikolajewicz U, Sterl A, Drijfhout SS (1999) Stochastically forced variability in the Antarctic Circumpolar Current. J Geophys Res 104(C5): 11049–11064

White WB, Cherry NJ (1999) Influence of the Antarctic circumpolar wave upon New Zealand temperature and precipitation during autumn–winter. J Climate 12: 960–976

White WB, Peterson RG (1996) An Antarctic circumpolar wave in surface pressure, wind, temperature and sea-ice extent. Nature 380: 699–702

Wolff JO, Maier-Reimer E, Legutke S (1997) The Hamburg Ocean Primitive Equation Model HOPE. Technical Report 13, German Climate Computer Center (DKRZ)